Spatial heterogeneity in liquid–liquid phase transition*

Yun-Rui Duan(段云瑞), Tao Li(李涛), Wei-Kang Wu(吴维康) Jie Li(李洁),
Xu-Yan Zhou(周戌燕), Si-Da Liu(刘思达), and Hui Li(李辉)†

Key Laboratory for Liquid-Solid Structural Evolution and Processing of Materials of Ministry of Education, Shandong University, Jinan 250061, *China*

(Received 24 October 2016; revised manuscript received 6 December 2016; published online 13 February 2017)

Molecular dynamics simulations are performed to investigate the liquid–liquid phase transition (LLPT) and the spatial heterogeneity in Al–Pb monotectic alloys. The results reveal that homogeneous liquid Al–Pb alloy undergoes an LLPT, separating into Al-rich and Pb-rich domains, which is quite different from the isocompositional liquid water with a transition between low-density liquid (LDL) and high-density liquid (HDL). With spatial heterogeneity becoming large, LLPT takes place correspondingly. The relationship between the cooling rate, relaxation temperature and percentage of Al and the spatial heterogeneity is also reported. This study may throw light on the relationship between the structure heterogeneity and LLPT, which provides novel strategies to control the microstructures in the fabrication of the material with high performance.

Keywords: spatial heterogeneity, liquid–liquid phase transition, phase separation

PACS: 64.70.Ja, 64.75.St, 64.60.My **DOI:** 10.1088/1674-1056/26/3/036401

1. Introduction

A possible first-order LLPT between two forms of the liquid phase in some supercooled pure substances has received considerable interest in recent years,[1–8] because LLPT offers an avenue for interesting applications that exploits different properties of distinct liquid phases.[9] Understanding LLPT and its dynamic properties is of great importance to researchers in the field of physics, chemistry and materials science. However, despite intense scrutiny over the years, scientists are still far from reaching a coherent understanding of unusual structural behavior in the process of LLPT.[10–12] The existence of two coexisting liquids with the same composition but different structure[13,14] has been a controversial issue.

Among the substances having two coexisting liquids in supercooled states are water,[5–8] silicon,[2] germanium,[15] carbon, and hydrogen, etc. There is much evidence from simulation and experiment results that is suggestive of the existence of LLPT for a variety of liquids. For example, the LLPT of water was first put forward[5] to account for its peculiar thermodynamic and dynamic anomalies in supercooled liquid states, which was followed by various theories[16–20] to support it. Recent studies provided sufficient evidence for a liquid–liquid transition in ST2 model[21–26] and TIP4P/2005 model[27–29] which gave the best agreement with the experiment among the TIPnP family of water.[30] Remarkably similar to water, The LLPT in Si was first predicted by Aptekar,[15] and subsequently supported by MD simulations combined with experiment data obtained by x-ray diffraction and Raman spectroscopy.[31–34] In addition, the coexistence of two forms of phosphorus liquids was directly observed by *in situ* x-ray diffraction experiment.[35–37] Besides the isocompositional LLPTs, supercooled liquid to liquid transition, especially in sulfur, has also been comprehensively studied.[38–40] However, to our limited knowledge, fewer efforts have been focused on the type of binary liquids in the perspective of LLPT, such as liquid Al–Pb binary alloy.

Considerable efforts have been devoted to studying the local structure in LLPT because the local structure leads to its heterogeneity which has close relation with the structural origins of LLPT and associated phenomena. For example, Debenedetti pointed out that the difference between two water liquids lies in their local structures: in the high density liquid, the local tetrahedrally coordinated hydrogen-bond structure is not fully developed, whereas in the low density liquid, locally "ice-like" hydrogen-bond network is fully realized.[5,9] The low density liquid had a more open network compared to the high density liquid. The two types of liquid phases separated by a line of first-order LLPT were identified by their density and local atomic structure. Tanaka also argued that liquid is not homogeneous and the heterogeneity may be responsible for the LLPT in the molecular liquid.[41] Subsequently, by defining parameters presenting the local favored heterogeneous structure, Tanaka gave a good explanation of LLPT in water.[42–44] By analogy with different structures of two forms of liquid in water, LLPT of liquid Si also involves structure transition from a metallic dense-packed structure at high temperature to a semiconducting open network at low temperature.[45] Furthermore, Treacy and Borisenko[46] believed that the continuous random network (CRN) model represents the structural topology of amorphous silicon which has

*Project supported by the National Natural Science Foundation of China (Grant No. 51271100), the National Basic Research Program of China (Grant No. 2012CB825702), and the Special Funding in the Project of the Taishan Scholar Construction Engineering.

†Corresponding author. E-mail: lihuilmy@hotmail.com

© 2017 Chinese Physical Society and IOP Publishing Ltd

been used successfully to liquid silicon to find the inhomogeneous paracrystalline structures containing local structure at the 10 to 20 angstrom length scale, indicating the structural heterogeneity. However, the relationship between structure heterogeneity and LLPT process remains uncertain. In addition, how to quantify structure heterogeneity remains unsolved.

Al–Pb alloy is essential for a number of industrially important materials, such as wheel bearings. However, its potential applications[47] are seriously limited because of a major drawback caused by two liquid phases within the miscibility gap having different densities, resulting in phase separation at the macro scale.[48,49] The existence of LLPT in alloy has important implications for understanding the low-temperature liquid state in general.[50,51] It may provide an opportunity for comprehensive and satisfactory understanding of the structures and properties of immiscible liquid alloy. Till now, although there has been much progress in the understanding of the behavior of phase separation, some important questions on the LLPT of binary alloy have remained unanswered.[52–55] In this paper, we report molecular dynamic simulations on the LLPT of Al–Pb alloy, highlighting its relationship with structure heterogeneity.

2. Model and simulation methods

In this study, MD simulations are used to investigate the structure of liquid Al–Pb alloy containing 10000 atoms placed between two isolated and smooth walls, initially arranged into $50 \times 50 \times 1$ face-centered cubic (FCC) lattice. The interaction among metal atoms is described with embedded-atom method (EAM) which is particularly appropriate for metallic systems. The directions x and y are imposed periodic boundary conditions, while the z direction is bounded with walls. In this work, we use MD package LAMMPS to perform the simulations. All simulations are carried out at a constant lateral pressure, using the constant number, lateral pressure, temperature (NPT) ensemble. The Nose–Hoover thermostat and barostat are used to control the temperature and pressure, respectively, and the velocity–verlet algorithm is used to integrate the equations of motion with a time step of 1 fs. The liquid is equilibrated at 2000 K first. Subsequently, the well-equilibrated liquid alloy is cooled from 2000 K to the target temperature at different quenching rates. The final structures are obtained after a relaxation process at the target temperature.

3. Results and discussion

3.1. Effect of the cooling rate on spatial heterogeneity

Figures 1(a) and 1(b) present snapshots of $Al_{50}Pb_{50}$ alloy in different cooling processes (i.e. 100, 10, 1, and 0.1 K/ps). As temperature decreases, Al atoms prefer to unite with Al atoms to form some island-like local Al-rich domains in an ocean of Pb-rich domains. Subsequently, Al-rich domains with different radii and shapes contact with each other to grow up as a bigger one. Meanwhile, the Al-rich domains evolve from irregular to round. Eventually, the homogeneous one single liquid phase transforms into two liquid phases with different components and densities, which is considered as a kind of LLPT. That is to say, phase separation takes place during the LLPT for Al–Pb monotectic alloy, which is quite different from the transformation between LDL and HDL in isocompositional liquid Si[2] and water.[6] It also differs from layering transitions induced by confinement and pressure in nanoconfined liquid.[56] It can be seen that, during the LLPT, Al-rich domains try to connect with each other to avoid meeting Pb-rich domains. As we know, for a given area, the circle has the smallest circumference. Therefore, the shape transformation from the irregular to the round is also an effective way for the Al-rich domains to avoid meeting the Pb-rich domains. Interface length between Al- and Pb-rich domains which is roughly estimated by the number of interface atoms is displayed in Fig. 1(c), exhibiting that the interface length decreases during the LLPT process. It can be deduced that the interface energy between Al- and Pb-rich domains is very high which makes the system reduce the interface length as much as it possibly could. Therefore, interface tension plays a non-negligible role in the LLPT process. It is worth noting that there are still some Al or Pb atoms dispersed in Pb- or Al-rich domains, attributing to the role of mixing configuration entropy, which can be expressed as

$$\Delta S_{\text{mix}} = -R(X_{\text{A}} \ln X_{\text{A}} + X_{\text{B}} \ln X_{\text{B}}),$$

where S_{mix} is the mixing configuration entropy, R is the gas constant, X_{A} and X_{B} is the molar fraction of component A and B. Taking a derivative with respect to X_{A}, it can be seen that when X_{A} is close to 0 or 1, its derivative would be approximate to infinity, meaning that obtaining pure Al or Pb needs to overcome a sharp decrease of entropy. Therefore, Al- or Pb-rich domains containing some number of Pb or Al atoms are thermodynamically stable.

Figure 1(b) shows that when the cooling rate is 100 K/ps, there is no noticeable phase separation. In contrast, when the cooling rate is 0.1 K/ps, obvious phase separation has taken place at 1600 K and the LLPT proceeds fast with the decreasing temperature. At 1200 K, two Al-rich island-like round domains exist in Pb-rich domain oceans, suggesting an obvious phase separation. The situations at 1 K/ps and 10 K/ps fall somewhere in the middle of 0.1 K/ps and 100 K/ps. It is understandable that higher cooling rate makes the atoms have not enough time to diffuse to complete phase separation before the system reaches the target temperature, while at lower cooling rate, atoms have enough time to diffuse and are free to couple or decouple with each other to finish the phase separation.

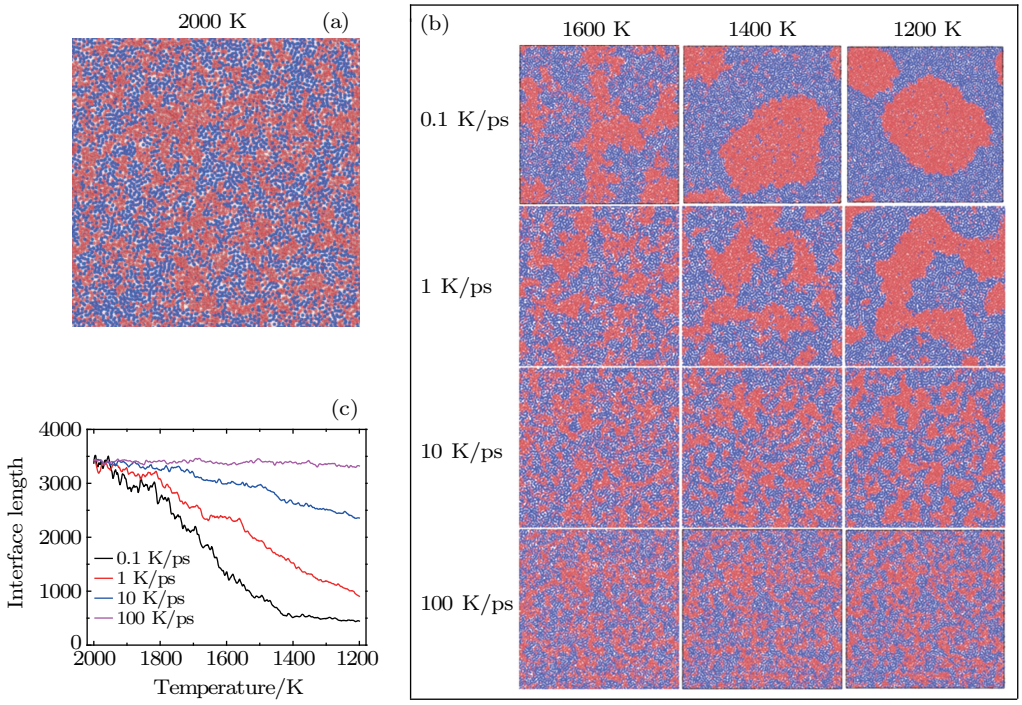


Fig. 1. (color online) (a) Initial structure of $Al_{50}Pb_{50}$ alloy at 2000 K. Al atoms are marked red and Pb atoms are marked blue. (b) Snapshots of $Al_{50}Pb_{50}$ alloy during the cooling process at four different cooling rates (i.e. 100, 10, 1 and 0.1 K/ps). (c) The interface length between the Al-rich domains and the Pb-rich domains during different cooling processes. The interface length is roughly estimated by the number of interface atoms.

It was found in liquid carbon film[57] that the position of the first peak gradually increased as the temperature decreased, which was opposite to the scenario of the normal substance. The author ascribed the anomaly to the LLPT, during which carbon transformed from the twofold coordinated liquid to the threefold coordinated liquid. Remarkably similar to carbon, the partial Al–Pb pair correlation function (PCF) during cooling process also exhibits the anomaly that the position of the first peak increases with the reduced temperature, as shown in Fig. 2(a). Moreover, the height of main peak declines notably as the temperature decreases, which is also contrary to the normal substance. The reason is that as temperature decreases, LLPT takes place. Moreover, Al atoms aggregate with Al atoms and separate with Pb atoms, so the first neighbor distance between Al and Pb atoms becomes large, corresponding to the shift to the right for the position of first peak. Furthermore, the possibility of finding a Pb atom around an Al atom decreases due to the separation of Al-rich domains with Pb-rich domains, corresponding to the decline of main peak. Obviously, the height of Al–Pb PCF main peak can give an indication of the extent of phase separation. If the phase separation degree is high, main peak of partial Al–Pb PCF would be low. When liquid $Al_{50}Pb_{50}$ alloy is cooled down at different cooling rates, the partial Al–Pb PCF at 1200 K is exhibited in Fig. 2(b), revealing that the lower cooling rate corresponds to lower main peak, thus, higher extent of phase separation, which shows favorable agreement with Fig. 1. Therefore, higher cooling rate is not helpful for phase separation.

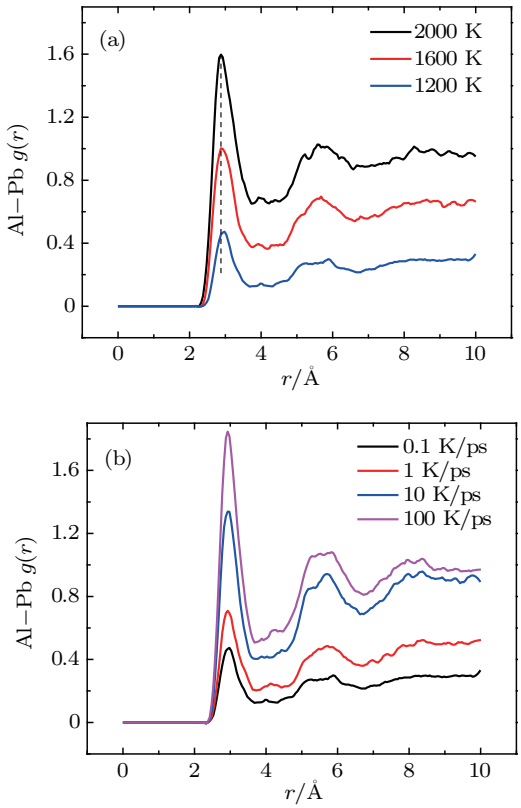


Fig. 2. (color online) (a) Al–Pb partial pair correlation function for $Al_{50}Pb_{50}$ alloy during the cooling process at the cooling rate of 0.1 K/ps. (b) Al–Pb pair correlation function at 1200 K during different cooling processes.

It is suggested that if the distance between two atoms is less than a given cutoff distance, which is equal to the position of the first minimum in the corresponding pair correlation

function, then the pair of atoms is considered to form a bond. Based on this principle, Al–Pb bond fraction at different cooling processes is calculated and displayed in Fig. 3(a), which displays the degree of Al atoms to meet the Pb atoms. As a consequence, Al–Pb bond fraction can be adopted as a measure of the degree of phase separation.

To well describe spatial heterogeneity in the LLPT process, micro-structure factor (MSF) is put forward and defined as follows:

$$\mathrm{MSF} = \sum_{i=1}^{N} \frac{(x_i - x)^2}{N},$$

where x_i is the atomic concentration of atom i, which is calculated by counting the number of Pb atoms and Al atoms within a distance of 6.5 Å around atom i. The quotient of the number of Pb atoms to the number of all atoms is exactly x_i. x is the average atomic concentration. N is the number of atoms. Based on the definition, figure 3(b) illustrates MSF at different cooling processes.

The definition of MSF is similar to the variance in mathematics, which is the expectation of the squared deviation of a random variable from its mean, and informally measures how far a set of random numbers are spread out from their mean. Similarly, the MSF is used to measure how far the concentration of each atom deviates from the average concentration. If the system tends to be homogeneous, then the concentration of each atom deviates little from the average, and MSF value is small. However, when the system displays a great degree of heterogeneity, the concentration of each atom deviates far from the average, and MSF value is large. Therefore, the MSF is effective to measure the extent of heterogeneity of liquid alloy.

Figure 3(a) shows that Al–Pb bond fraction drops with decreasing temperature, suggesting that Al atoms are unwilling to meet Pb atoms to form a bond during phase separation. Meanwhile, as temperature reduces, the MSF curve rises, as shown in Fig. 3(b), revealing that spatial heterogeneity increases during phase separation. Furthermore, Al–Pb bond fraction curve and MSF curve are highly correlated. For example, when Al–Pb bond fraction curve drops fast, the corresponding MSF curve drops fast too. It can be concluded that as spatial heterogeneity becomes larger, the LLPT takes place correspondingly.

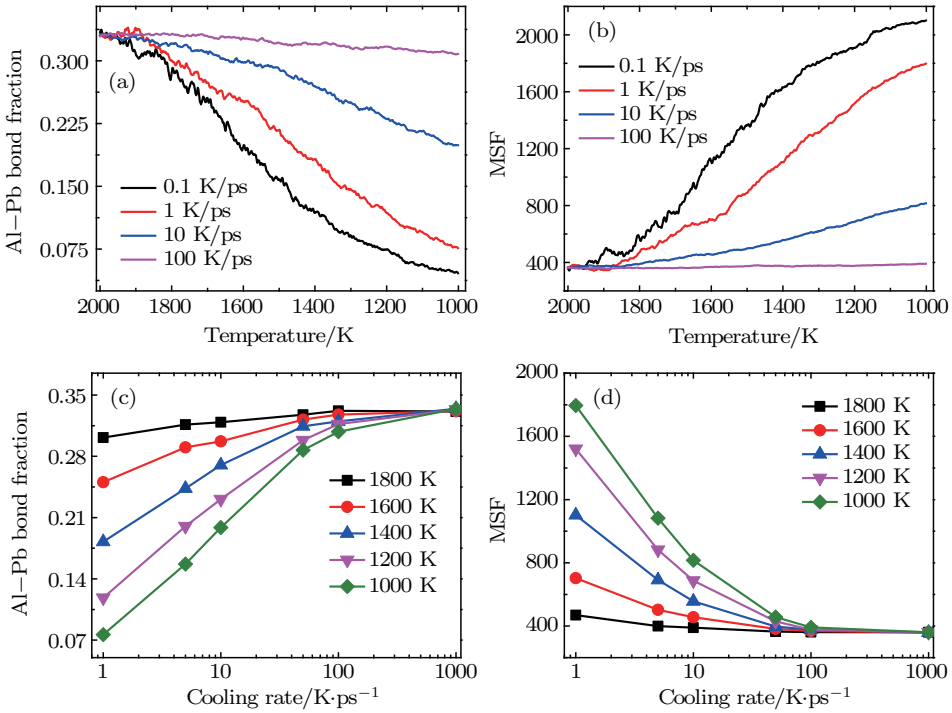


Fig. 3. (color online) (a) Al–Pb bond fraction and (b) MSF of $Al_{50}Pb_{50}$ alloy during different cooling processes. If the distance between two atoms is less than a given cutoff distance, which is equal to the position of the first minimum in the appropriate pair correlation function, then the pair of atoms is considered to form a bond. (c) Al–Pb bond fraction and (d) MSF as a function of cooling rate at different temperatures of cooling process.

The parameter to judge the start of the LLPT in water was the density as reported by Wang *et al.*[58] By detecting the average density of water with warming and cooling scans, the author recognized the position where the maximum density difference between the cooling and warming scans emerged as the starting position of LLPT. Similarly, there is also a parameter MSF to determine the start of the LLPT of Al–Pb alloys. It is understandable that there is a striking close relation between the LLPT and the spatial heterogeneity. Note that MSF curve has a period of fluctuation without apparent rise or drop at the initial stage of the cooling process. The starting temperature where MSF rises can be considered apparently as

the starting temperature point of LLPT. It can be seen from Fig. 3(b) that when the cooling rates are 0.1 K/ps, 1 K/ps, and 10 K/ps, LLPT starts to take place at 1950 K, 1880 K, and 1850 K respectively. Interestingly, the three starting temperature points are also exactly located on the points where Al–Pb bond fraction curves start to drop apparently at the corresponding cooling rates. The good consistency is suggested that MSF is a valid parameter to determine the start of the LLPT. Obviously, LLPT begins to take place at higher temperature if the cooling rate is low. The reason is that diffusion is necessary to the nucleation and phase transition. However, if the cooling rate is high, atoms are unable to diffuse in time and LLPT is delayed to the lower temperature. Therefore, high cooling rate is unfavorable to the formation of LLPT.

Next, we compare Al–Pb bond fraction and MSF curves at different cooling rates. When the cooling rate is 100 K/ps, both Al–Pb bond fraction and MSF values exhibit no dramatic change, suggesting low extent of phase separation and spatial heterogeneity; whereas when the cooling rate is 0.1 K/ps, both Al–Pb bond fraction and MSF values show dramatic change, indicating high extent of phase separation and spatial heterogeneity. To directly investigate how cooling rate affects the LLPT process and spatial heterogeneity, we plot Al–Pb bond fraction and MSF curves as a function of cooling rate as displayed in Figs. 3(c) and 3(d). It can be seen that at the fixed temperature, Al–Pb bond fraction and MSF change monotonically with the cooling rate. Higher cooling rate tends to cause a lower extent of phase separation and spatial heterogeneity. Moreover, the slope of both curves at higher cooling rate is steeper than that at lower cooling rate, suggesting that LLPT forming rate is higher at lower cooling rate than that at high cooling rate. Therefore, high cooling rate has a detrimental effect on the LLPT and spatial heterogeneity.

3.2. Effect of the relaxation temperature on spatial heterogeneity

To explore how relaxation temperature affects the spatial heterogeneity, the liquid alloys are quenched to the target temperature at 100 K/ps and then relaxed at the target temperature. Since MSF is effective to estimate the spatial heterogeneity, figure 4(a) illustrates MSF curves at 1 ns when the liquid alloys are equilibrium state. For liquid $Al_{90}Pb_{10}$, $Al_{75}Pb_{25}$, $Al_{65}Pb_{35}$, and $Al_{50}Pb_{50}$ alloys, MSF curves rise first with the decreasing temperature and start to drop after 1200 K, meaning that MSF reaches its maximum value at 1200 K. However, the MSF of liquid $Al_{35}Pb_{65}$ alloy is another case where its MSF reaches maximum at 1100 K. For liquid $Al_{25}Pb_{75}$ and $Al_{10}Pb_{90}$ alloys, MSF rises monotonically with decreasing temperature.

Another important issue is the reaction rate of the LLPT at different temperatures. Contrary to the conventional wisdom that the reaction rate is higher at higher temperature, our results reveal an opposite trend in terms of LLPT process. Figure 4(b) shows MSF curves at different temperatures during the relaxation process for $Al_{50}Pb_{50}$ alloy. If the spatial heterogeneity changes fast, the reaction rate is considered to be high. Therefore, we can judge the reaction rate from the slope of MSF curves. It can be seen that the slope of MSF curve at lower temperature is larger than that at higher temperature, which proves that lower temperature leads to higher reaction rate.

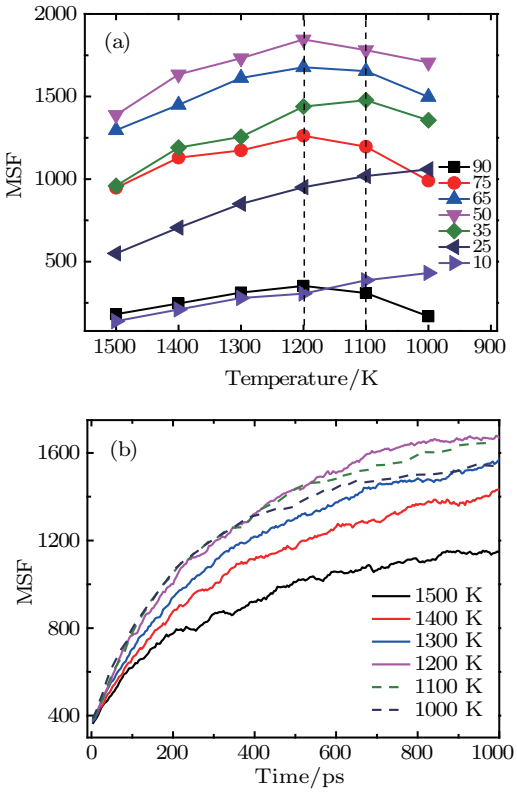


Fig. 4. (color online) (a) MSF versus temperature at 1000 ps in relaxation process for alloys with different atomic Al percentages. (b) MSF of $Al_{50}Pb_{50}$ alloy during relaxation process.

Through the example of liquid $Al_{50}Pb_{50}$ alloy, we explain the reason why MSF curves behave like this. Figure 5(a) shows the final equilibrium structures in the relaxation process under different temperatures. At 1500 K, the numbers of Al atoms dispersed in Pb-rich domains and Pb atoms dispersed in Al-rich domains are both large. As temperature decreases, the numbers of Al atoms dispersed in Pb-rich domains and Pb atoms dispersed in Al-rich domains both reduce remarkably. It might be understood that the state of Al atoms aggregating with Al atoms and Pb atoms aggregating with Pb atoms is thermodynamically stable. However, the atoms at higher temperature can easily overcome the bound from homogeneous atoms and jump to the heterogeneous atoms group owing to their higher kinetic energy. As a consequence, the structure at lower temperature deviates further from its initial homogeneous state, which suggests that the lower temperature leads

to a higher MSF value and further results in high spatial heterogeneity at the temperature range from 1500 K to 1200 K. Similarly the final equilibrium state at lower temperature deviates further from initial relative homogeneous state than that at higher temperature, the driving force to increase the spatial heterogeneity is stronger at lower temperature. Therefore, spatial heterogeneity rises faster at lower temperature, thus reaction rate is higher at lower temperature than that at higher temperature. It can be seen from Fig. 5(b) that, at 1200 K, both Al-rich domains and Pb-rich domains are disordered liquid, whereas Al-rich domains start to crystallize at 1100 K because Al has a higher melting point and is more prone to crystallize than Pb. The LLPT is unable to proceed adequately because atom diffusion is largely impeded by the crystallization of the Al-rich domains, which can account for the fact that spatial heterogeneity at 1100 K is smaller than that at 1200 K. Figure 5(c) illustrates the partial Al–Al PCF of relaxation equilibrium state which can further support the explanation. At 1200 K or above, the short and broad second and third peaks support the fact that Al-rich domains are liquid. Meanwhile, at 1100 K, the second and third peaks become narrow and high, forming an ordered crystal of Al-rich domains. In terms of liquid $Al_{90}Pb_{10}$, $Al_{75}Pb_{25}$, $Al_{65}Pb_{35}$, and $Al_{50}Pb_{50}$ alloy with high Al percentage, the diffusion impediment due to crystallization has already become very large at 1100 K, so the MSF maximum emerges at 1200 K. As the Al percentage decreases, the effect of crystallization of Al-rich domains becomes weaker and weaker. So, for the liquid $Al_{35}Pb_{65}$ alloy, the impediment is not obvious even at 1100 K, and the MSF reaches its maximum at 1100 K, thus, the spatial heterogeneity reaches its maximum. Therefore, when the alloys are liquid, the spatial heterogeneity increases with the decreasing temperature. As the temperature is further reduced, the spatial heterogeneity would decrease due to the crystallization of Al-rich domains. The temperature where the spatial heterogeneity maximum emerges would depend on the Al content.

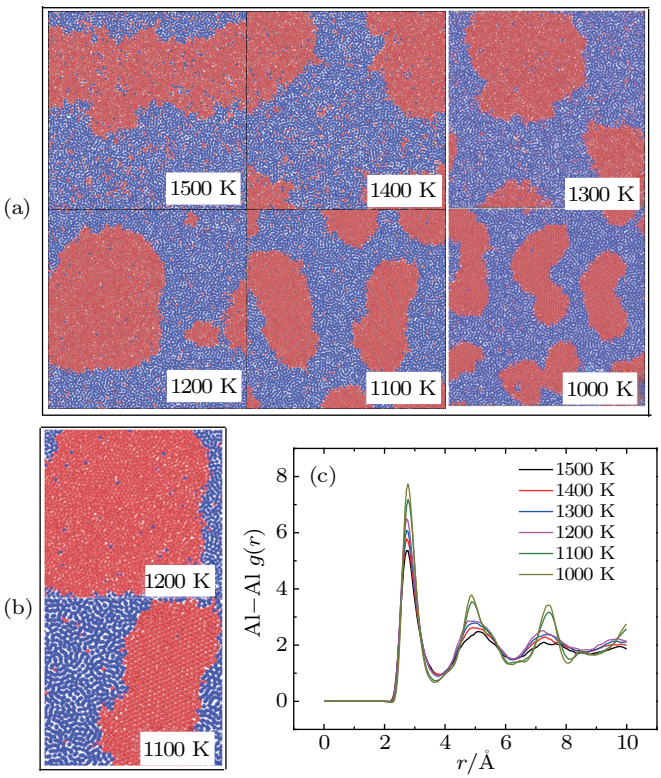


Fig. 5. (color online) (a) Structures of the $Al_{50}Pb_{50}$ alloy at different temperatures when the alloy is relaxed to its equilibrium state. (b) Enlarged Al-rich domains at 1200 K and 1100 K in panel (a), (c) Al–Al pair correlation function for $Al_{50}Pb_{50}$ alloy at its relaxation equilibrium state.

3.3. Effect of the Al percentage on the spatial heterogeneity

Finally we report the effect of Al percentage on the spatial heterogeneity during the LLPT process. Figure 6(a) shows the MSF during the relaxation process at 1300 K for all liquid alloys which are cooled from 2000 K at a cooling rate of 100 K/ps. During the relaxation process, $Al_{50}Pb_{50}$ alloy always has the largest MSF value, thus the largest spatial heterogeneity. If the Pb percentage goes away from 50%, the MSF value becomes smaller. Therefore, the spatial heterogeneity is strongly component-dependent. Moreover, the difference of MSF values between two adjacent time points for $Al_{50}Pb_{50}$ alloy is larger than that of these alloys whose atomic Al percentage is far from 50%, indicating that the spatial heterogeneity of $Al_{50}Pb_{50}$ changes faster than that of other alloys. That is to say, the reaction rate of $Al_{50}Pb_{50}$ alloy is larger than that of other alloys. The horizontal axis is divided into 20 component intervals and we count the number of atoms falling into every component interval when the system is at relaxation equilibrium state as shown in Fig. 6(b). It can be found that the components of most atoms are located at 0–10% and 90%–100%, corresponding to the Al-rich domains and Pb-rich domains, regardless of Al percentage. Therefore, the initial homogeneous structure of the liquid $Al_{50}Pb_{50}$ alloy at 2000 K deviates further from the final equilibrium state compared to other alloys, leading to the largest MSF value of $Al_{50}Pb_{50}$ alloy. Moreover, the driving force to increase the spatial heterogeneity of the $Al_{50}Pb_{50}$ alloy is also larger than that of other alloys. So the reaction rate of the $Al_{50}Pb_{50}$ alloy is also the largest. In conclusion, $Al_{50}Pb_{50}$ alloy has the largest spatial heterogeneity and reaction rate, which are strongly component-dependent.

Wang *et al.*[58] plotted a phase diagram of the LLPT of the confined heavy water by finding critical points under different pressures and temperatures. By the same token, phase diagram of the LLPT in the confined liquid SiC was also plotted.[56] Here, we calculate the MSF of all alloys during the cooling process when the cooling rate is 1 K/ps. By determining the starting point where the MSF values start to rise conspicuously, we plot the phase diagram of the LLPT of the Al–Pb

alloy compared with that obtained by previous study[59] which is shown in Fig. 6(c). The starting temperature of our study is higher than that of the previous study, which may result from the potential function. However, the trend of the two curves is similar, indicating that our result is valid. Through the phase diagram, we can read the temperature where LLPT starts to take place for alloys of any components.

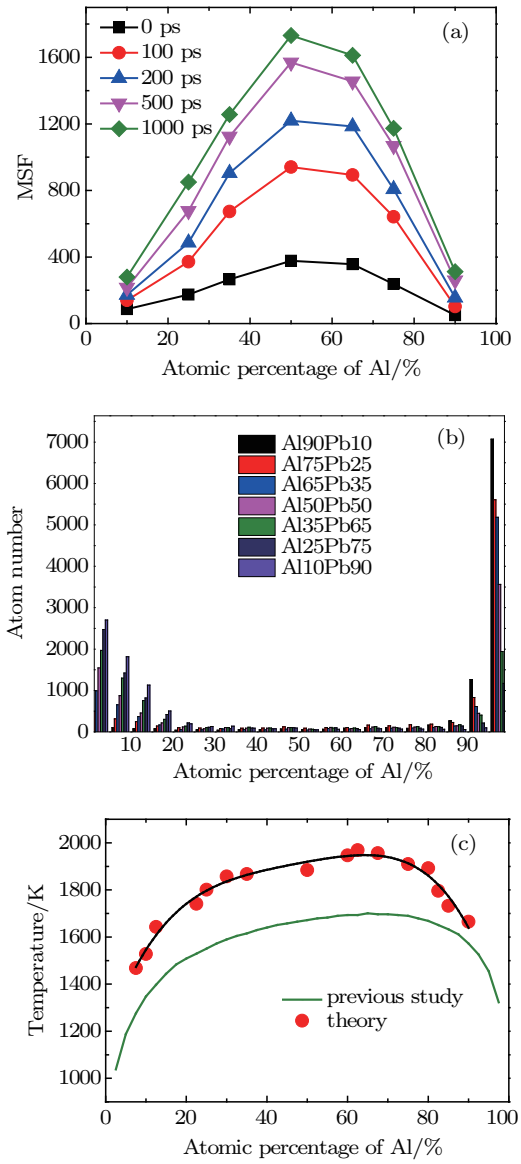


Fig. 6. (color online) (a) MSF as a function of component at different relaxation time. (b) The number of atoms distributed in each component interval when the system is at relaxation equilibrium state. (c) The phase diagram for Al–Pb monotectic liquid alloy. Previous study data are taken from Ref. [59].

4. Conclusion and perspectives

In summary, molecular dynamics simulations are carried out to investigate the liquid–liquid phase transition (LLPT) and the spatial heterogeneity in Al–Pb monotectic alloys. It is shown that the homogeneous one single liquid phase transforms into two liquid phases with different components and densities, which is considered as a type of LLPT. LLPT process is highly correlated with the spatial heterogeneity. With increasing spatial heterogeneity, LLPT takes place correspondingly. Higher cooling rate can delay the LLPT and prevent the increase of spatial heterogeneity. Spatial heterogeneity would increase with decreasing temperature when the alloys are liquid. As the temperature further reduces, spatial heterogeneity would decrease due to the crystallization of Al-rich domains. Moreover, high temperature can lead to low LLPT reaction rate. Spatial heterogeneity and LLPT reaction rate are strongly component-dependent. Of all alloys, $Al_{50}Pb_{50}$ alloy has the largest spatial heterogeneity and reaction rate. Specifically, the phase diagram of the LLPT of the Al–Pb alloy is plotted.

References

[1] Vasisht V V, Saw S and Sastry S 2011 *Nat. Phys.* **7** 549
[2] Sastry S and Angell C A 2003 *Nat. Mater.* **2** 739
[3] Angell C A 2008 *Science* **319** 582
[4] Speedy R J 1982 *J. Chem. Phys.* **86** 982
[5] Poole P H, Sciortino F, Essmann U and Stanley H E 1992 *Nature* **360** 324
[6] Mishima O and Stanley H E 1998 *Nature* **392** 164
[7] Wang W P, Liu F S and Zhang N C 2014 *Acta Phys. Sin.* **63** 126201 (in Chinese)
[8] Liu J, Wang S Y, Zheng C P, Xin L J, Wang D and Sun M H 2007 *Chin. Phys. Lett.* **24** 2025
[9] Kurita R, Murata K and Tanaka H 2008 *Nat. Mater.* **7** 647
[10] Debenedetti P G 2003 *J. Phys. Condens. Matter* **15** R1669
[11] Mishima O and Stanley H E 1998 *Nature* **396** 329
[12] Mallamace F, Broccio M, Corsaro C, Faraone A, Majolino D, Venuti V, Liu L, Mou C Y and Chen S H 2007 *Proc. Natl. Acad. Sci. U. S. A.* **104** 424
[13] Gibson H M and Wilding N B 2006 *Phys. Rev. E* **73** 061507
[14] Xu L, Buldyrev S V, Giovambattista N, Angell C A and Stanley H E 2009 *J. Chem. Phys.* **130** 054505
[15] Aptekar L 1979 *Sov. Phys. Dokl.* **24** 993
[16] Ponyatovskii E, Sinand V and Pozdnyakova T 1994 *ZhETFPisma Redaktsiiu* **60** 352
[17] Moynihan C T 1996 *J. Non-Cryst. Solids* **203** 359
[18] Poole P H, Sciortino F, Grande T, Stanley H E and Angell C A 1994 *Phys. Rev. Lett.* **73** 1632
[19] Borick S S, Debenedetti P G and Sastry S 1995 *J. Chem. Phys.* **99** 3781
[20] Tejero C F and Baus M 1998 *Phys. Rev. E* **57** 4821
[21] Sciortino F, Saika-Voivod I and Poole P H 2011 *Phys. Chem. Chem. Phys.* **13** 19759
[22] Liu Y, Palmer J C, Panagiotopoulos A Z and Debenedetti P G 2012 *J. Chem. Phys.* **137** 214505
[23] Kesselring T A, Lascaris E, Franzese G, Buldyrev S V, Herrmann H J and Stanley H E 2013 *J. Chem. Phys.* **138** 244506
[24] Poole P H, Bowles R K, Saika-Voivod I and Sciortino F 2013 *J. Chem. Phys.* **138** 034505
[25] Palmer J C, Martelli F, Liu Y, Car R, Panagiotopoulos A Z and Debenedetti P G 2014 *Nature* **510** 385
[26] Smallenburg F and Sciortino F 2015 *Phys. Rev. Lett.* **115** 015701
[27] Abascal J L and Vega C 2010 *J. Chem. Phys.* **133** 234502
[28] Russo J and Tanaka H 2014 *Nat. Comm.* **5** 3556
[29] Sumi T and Sekino H 2013 *RSC Adv.* **3** 12743
[30] Vega C, Abascal J L, Conde M and Aragones J 2009 *Faraday Discuss.* **141** 251
[31] Deb S K, Wilding M, Somayazulu M and McMillan P F 2001 *Nature* **414** 528
[32] McMillan P F, Wilson M, Daisenberger D and Machon D 2005 *Nat. Mater.* **4** 680
[33] Daisenberger D, Wilson M, McMillan P F, Cabrera R Q, Wilding M C and Machon D 2007 *Phys. Rev. B* **75** 224118
[34] Daisenberger D, Deschamps T, Champagnon B, Mezouar M, Quesada Cabrera R l, Wilson M and McMillan P F 2011 *J. Phys. Chem. B* **115** 14246

[35] Katayama Y, Mizutani T, Utsumi W, Shimomura O, Yamakata M and Funakoshi K 2000 *Nature* **403** 170
[36] Monaco G, Falconi S, Crichton W and Mezouar M 2003 *Phys. Rev. Lett.* **90** 255701
[37] Katayama Y, Inamura Y, Mizutani T, Yamakata M, Utsumi W and Shimomura O 2004 *Science* **306** 848
[38] Zhang D D, Liu X R, He Z and Hong S M 2016 *Chin. Phys. Lett.* **33** 026301
[39] Zhang D D, Liu X R, Hong S M, Li L B, Cui K P, Shao C G, He Z and Xu J A 2014 *Chin. Phys. Lett.* **31** 066401
[40] Tang F, Zhang L J, Liu F L, Sun F, Yang W G, Wang J L, Liu X R and Shen R 2016 *Chin. Phys. B* **25** 046102
[41] Tanaka H 2000 *Phys. Rev. E* **62** 6968
[42] Tanaka H 2000 *J. Chem. Phys.* **112** 799
[43] Tanaka H 2000 *Europhys. Lett.* **50** 340
[44] Tanaka H 2012 *Eur. Phys. J. E* **35** 1
[45] Poole P H, Grande T, Angell C A and McMillan P F 1997 *Science* **275** 322
[46] Treacy M and Borisenko K 2012 *Science* **335** 950
[47] Ratke L and Diefenbach S 1995 *Mater. Sci. Eng. R.* **15** 263
[48] Ohnuma I, Saegusa T, Takaku Y, Wang C, Liu X, Kainuma R and Ishida K 2009 *J. Electron. Mater.* **38** 2
[49] Shi R P, Wang C P, Wheeler D, Liu X J and Wang Y 2013 *Acta Mater.* **61** 1229
[50] Cao C D 2006 *Chin. Phys. B* **15** 872
[51] Ma C, Dou Z Y, Zhu H Y, Fu G Y, Tan X, Bai B, Zhang P C and Cui Q L 2016 *Chin. Phys. B* **25** 046401
[52] Zhang X M, Wang W L, Ruan Y and Wei B B 2010 *Chin. Phys. Lett.* **27** 026401
[53] Cao C D and Görler G P 2005 *Chin. Phys. Lett.* **22** 482
[54] Li Z Q, Wang W L, Zhai W and Wei B B 2011 *Acta Phys. Sin.* **60** 108101 (in Chinese)
[55] Yan N, Wang W L, Dai F P and Wei B B 2011 *Acta Phys. Sin.* **60** 036402 (in Chinese)
[56] Wu W, Zhang L, Liu S, Ren H, Zhou X and Li H 2016 *J. Am. Chem. Soc.* **138** 2815
[57] He Y, Li H, Jiang Y, Li X and Bian X 2014 *Sci. Rep.* **4** 3635
[58] Wang Z, Ito K, Leão J B, Harriger L, Liu Y and Chen S H 2015 *J. Phys. Chem. Lett.* **6** 2009
[59] Bale C W and Bélisle E *Fact-Web Suite of Interactive Programs*, www.factsage.com